Chiral zero-energy modes in the disordered α-T_3 lattice

Han-Lin Liu and J. Wang*
School of Physics, Southeast University, Nanjing 210096, China

Jun-Feng Liu†
School of Physics and Materials Science, Guangzhou University, Guangzhou 510006, China

(Received 6 December 2022; revised 13 February 2023; accepted 21 February 2023; published 16 March 2023)

The α-T_3 lattice is an interpolate between the graphene ($\alpha = 0$) and the Dice lattices ($\alpha = 1$) and has a nondispersive flat band across the Dirac bands at the band center ($E = 0$). In this paper, we study the delocalization effect of the additional chiral zero-energy modes (CZEM) from the vacancy disorder in the α-T_3 lattice and address the influence of the flat band on the CZEM. It is shown that the mere broadening of the flat band without the CZEM could produce a supermetallic phase around the band center $E \sim 0$ as well as an adjoined narrow localization regime. When the CZEM from the vacancy disorder is turned on, the transport property resembles the graphene case ($\alpha = 0$) that electrons in the low-energy regime are fully localized except the Dirac point of $E = 0$, which is a critical delocalization point because the zero-energy conductivity (ZEC) is independent of the inelastic-scattering strength η. But the ZEC itself is shown to weakly rely on both the model parameter α and the vacancy density n_c due to the broadening effect of the flat band. The extreme vacancy imbalance among each ABC site of a primitive cell is also studied, and the electron transport around $E \sim 0$ is changed to be either the pure inelastic disorder case without vacancy or the fully localized phase without the critical delocalization point of $E = 0$, which depends on the central site B atom replaced by vacancy or not.

DOI: 10.1103/PhysRevB.107.125412

I. INTRODUCTION

The flat band system [1–6] has received much attention for the past decade, especially, since the discovery of the superconductivity in the twisted bilayer graphene [7,8] where a nearly flat band was identified around the magic angle. Due to the destructive quantum interferences, the electron group velocity is exactly zero for the flat band so that the kinetic energy is quenched, and the electron density of states are divergent, which together with the Coulomb interaction may give rise to some peculiar quantum phases, such as ferromagnetism [9–12], high-temperature superconductivity [13,14], zero-field fractional quantum Hall effect [15,16], Bose-Einstein condensation [17], Wigner crystallization [18], etc.

The formation of the flat band generally originates from the lattice with a chiral sublattice symmetry and an imbalance among the number of sublattice sites [1], i.e., the flat band due to the extra hub atom is usually accompanied by the linear Dirac bands due to the chiral symmetry. The study of the flat band has a long history, some materials with a perfect flat band and absolute zero-energy dispersion have been proposed in the literature, such as the Dice [19] or Lieb lattice [20], and they have been demonstrated in the optical lattice systems [21–26] until recent years. A more robust flat band was also identified in the 1T-TaS_2 [27,28] material that can survive from the spin-orbit interaction. In bis(iminothiolato)nickel monolayer lattice [29,30], the flat band was shown crossing the single Dirac band at the band center.

The flat band is supposed not to directly contribute to the electron transport because the electrons are fully localized with a zero group velocity, however, the electrons in the neighboring (crossed) bands can exhibit some remarkable properties. For example, the α-T_3 lattice model [31–36], an interpolate between the graphene lattice ($\alpha = 0$) and the Dice ($\alpha = 1$) lattice, has shown the super-Klein tunneling [37,38] and supercollimation phenomena [39]. In addition, the conductivity of the α-T_3 lattice was extensively investigated, and there exists some controversy about the zero energy conductivity (ZEC), Louvet *et al.* [40] reported that there is a zero ZEC by the scattering wave-function method due to the existence of the flat band, but oppositely, Vigh *et al.* [41] showed a divergent ZEC in the Dice lattice by using the Kubo formula. The similar nonzero ZEC was also found in the Lieb lattice [42] and the line-centered honeycomb lattice system with a flat band [43].

In monolayer graphene, a universal ZEC $\sigma_0 = 4e^2/h\pi$ was found in both the pristine and the vacancy-disorder cases [44–47]. The vacancy disorder is believed to induce chiral zero energy modes (CZEM) whereas the chiral symmetry of the system is untouched [48,49]. Since the time-reversal symmetry, and spin-rotation symmetries are also invariant, the vacancy-disordered graphene belongs to the chiral orthogonal (BDI) class. Ferreira and Mucciolo [47], by means of accurate large-scale numerical calculations, showed that zero energy is a critical delocalization point because the ZEC is

*jwang@seu.edu.cn
†phjfliu@gzhu.edu.cn

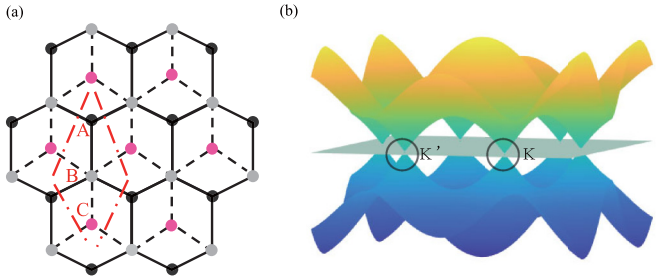

FIG. 1. (a) A schematic α-T_3 lattice with a primitive cell containing ABC atoms. The AB atoms constitute the basic honeycomb lattice with the C atom residing in the center of each hexagon. (b) The band structure of the α-T_3 lattice. The only one p_z orbit of each atom is considered, such as the graphene lattice, and there is an additional flat band across the Dirac points of K and K'.

independent of the inelastic-scattering strength η as well as the vacancy density. The similar phenomenon was also found in the chiral-unitary-class (AIII) and chiral-symplectic class (CII) two-dimensional (2D) semimetals of a square bipartite lattice system [50]. This motivates us to study the CZEM fate in the α-T_3 lattice as well as its interplay with the original zero-energy flat band.

In this paper, we numerically compute the low-energy conductivity of the α-T_3 lattice by using the Chebyshev polynomials Green's function (CPGF) method [47,51] and the Kubo-Greenwood conductivity formula. We show that a supermetallic phase occurs around the band center $E \sim 0$ together with an adjacent localized transport regime when the flat band is broadened merely by the inelastic scattering without the vacancy disorder or CZEM. Oppositely, the vacancy-disorder-induced CZEM can make the low-energy regime localized fully except the $E = 0$ point, which is referred to as the critical delocalization point the same as the graphene case. The ZEC magnitude is now independent of η but instead, dependent on the system parameter α as well as the vacancy density n_c due to the interplay of the CZEM and the broadened flat band. The extremity of the vacancy imbalance among different atom sites is also studied and the low-energy transport properties of the system would be drastically affected.

This paper is organized as follows. In Sec. II, we introduce the lattice model and the formula for calculating the conductivity. In Sec. III, numerical calculations of the density of states are presented. The conductivity without and with the vacancy disorder are calculated in Secs. IV and V, respectively. A brief conclusion is drawn in the last section.

II. MODEL AND FORMULA

We start from the α-T_3 lattice structure as schematically shown in Fig. 1(a), where the A and B sites comprise a honeycomb lattice whereas site C is introduced at the center of each hexagon to form the Dice lattice structure. The parameter α is reflected in the hopping energy of electrons between sites B and C, $t' = \alpha t$ with t, the hopping energy between A and B sites of the graphene lattice, whereas the hopping between A and Csites is prohibited. The prominent characteristic of the α-T_3 model is the zero-dispersion flat band crossing the two Dirac points of K and K' as shown in Fig. 1(b). The Hamiltonian of the α-T_3 model in the lattice representation reads

$$\mathcal{H} = \sum_{\langle ij\rangle} t c_i^\dagger c_j + \sum_{\langle jk\rangle} t' c_j^\dagger c_k, \tag{1}$$

where $c_{i,j,k}^\dagger$ ($c_{i,j,k}$) is the creation (annihilation) operator of electrons on the corresponding–C sites denoted by $\gamma = i, j, k$ indices, respectively. The first term is the electron hopping between A and B sites whereas the second one, $t' = \alpha t$, is that between B and C sites. The summation of $\langle ij\rangle$ ($\langle jk\rangle$) runs over the nearest-neighbor sites of AB (BC). The spin degree of freedom is degenerate by default and, thus, neglected here.

The conductivity σ of a finite-size sample is given by the Kubo-Greenwood formula [52,53]

$$\sigma(E) = \frac{2\hbar e^2}{\pi\Omega}\mathrm{Tr}[ImG_\eta(E)\hat{v}_x ImG_\eta(E)\hat{v}_x], \tag{2}$$

where $\hat{v}_x = \frac{1}{i\hbar}[\hat{x}, \mathcal{H}]$ is the velocity operator, Ω is the sample area, $G_\eta(E) = [E + i\eta - \mathcal{H}]^{-1}$ is the retarded Green's function, η is the level broadening factor representing an energy-independent inelastic-scattering strength.

The CPGF method [47,51] is employed to calculate the conductivity since it has already proven to be a powerful tool to study numerically the material conductivity [47], i.e., first-kind Chebyshev polynomials $\{T_n(x)\}$ (n, an integer) as a basis are employed to expand the Green's function, which reads

$$G_\eta(E + i\eta) = \frac{1}{W}\sum_{n=0}^{\infty} g_n(\epsilon, \eta) T_n(\hat{h}), \tag{3}$$

where $T_n(\hat{h})$ is defined though the Chebyshev recursion sequences: $T_0(\hat{h}) = I$, $T_1(\hat{h}) = \hat{h}$, and $T_{n+1}(\hat{h}) = 2\hat{h}T_n(\hat{h}) - T_{n-1}(\hat{h})$, $g_n(\epsilon, \eta)$ is the expanding coefficient, $\epsilon = E/W$, $\hat{h} = \mathcal{H}/W$ with W being the half bandwidth.

The system size in calculations is set as $N_s = 9000 \times 9000$, whereas the number of random vector N_R in selecting the original eigenvalue of $\mathcal{H}$ is generally set as $N_R = 50$. In fact, when the Fermi energy is far away from the Dirac point $E = 0$ or the η factor is not too small, N_R can be much smaller and even can be set as $N_R = 1$. The same situation occurs for the site random vacancy chosen in the lattice sample, and the sample average is taken as $r = 30$ in maximum, which sufficiently makes the results stable. The moment number of Chebyshev polynomial is taken as $N = 8000$, and it is related to the η factor $N \sim W/\eta$ to ensure the numerics convergence, where W is the half bandwidth $W = 3t\sqrt{1+\alpha^2}$. In numerics, $t = 1$ is set as the energy unit, and the temperature is taken zero. In addition, one cannot take a too small η in this CPGF method, which costs a very larger moment number and renders the time consumption of numerics impossible.

III. DENSITY OF STATES

Before we present the conductivity result, we first calculate the density of states (DOS) of electrons, which are given by

$$\nu(E) = \frac{-1}{N_s\pi}\mathrm{Tr}[ImG_\eta(E + i\eta)], \tag{4}$$

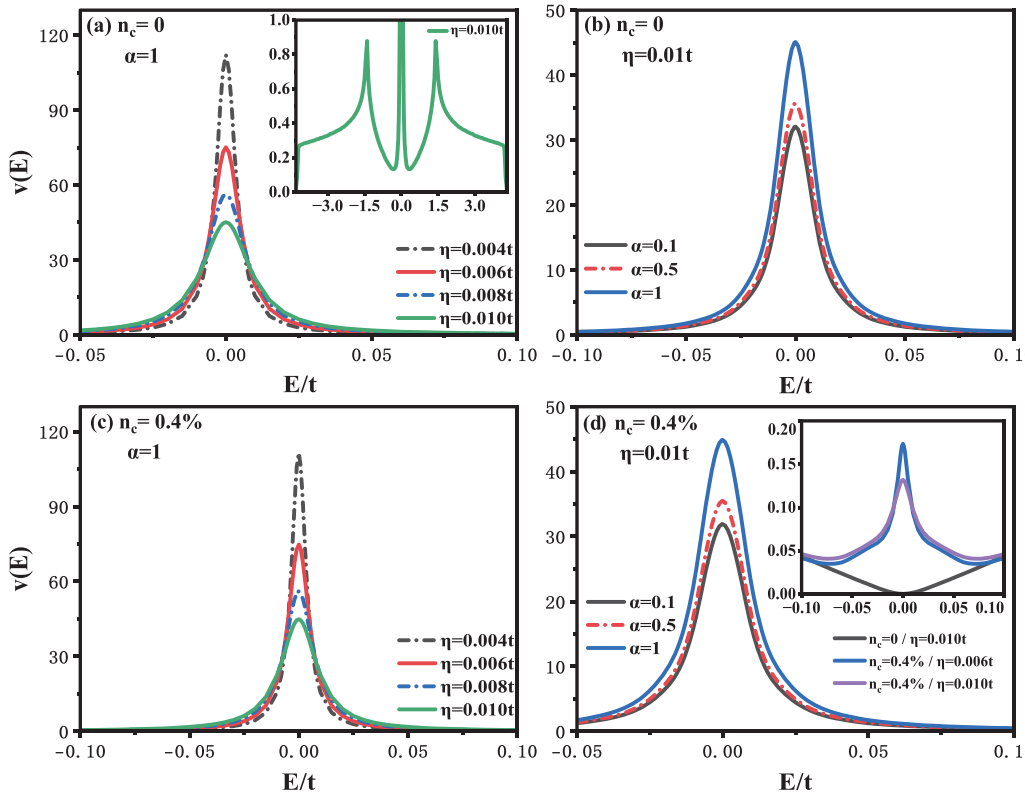

FIG. 2. Density of states $v(E)$ of the α-T_3 lattice for zero vacancy disorder cases in (a) and (b) and for nonzero vacancy cases in (c) and (d). Parameters are $\alpha = 1$ in (a) and (c) and $\eta = 0.01t$ in (b) and (d), the nonzero vacancy density $n_c = 0.4\%$. The inset in (a) is the DOS profile for the whole energy regime whereas the inset in (d) is the graphene DOS with $\alpha = 0$ with and without vacancy.

with N_s, the system size. The CPGF is efficient to calculate the DOS even for a much larger size sample. In Figs. 2(a) and 2(b), we present the DOS in the low-energy regime without any vacancy disorder. It is shown that the DOS exhibit an outstanding peak at the band center $E = 0$, this clearly stems from the broadened flat band due to the nonzero η, which mimics the inelastic scattering. The larger the η is, the much lower the DOS peak at $E = 0$ is. Although the parameter α can further enhance the DOS height at $E = 0$ since the flat band originates from the unbalanced atom $C$and α represents to some extent the weight of the flat band in the DOS of the α-T_3 lattice. In the inset of Fig. 2(a), the profile of the DOS in the whole band is shown for comparison. In addition, the sharp decrease in DOS with energy around $E = 0$ is a little similar to that induced by the Van Hove singularity in some special matrials [54].

In Figs. 2(c) and 2(d), the site vacancy is calculated with the density set as $n_c = 0.4\%$. Here, the vacancy disorder is uniformly distributed among the ABC sites of Fig. 1(a), and there is no bias for the site replacement. It is shown that the DOS do not exhibit much difference between the zero and the nonzero n_c cases by comparing Fig. 2(a) with Fig. 2(c). The vacancy is expected to induce the CZEM, which contributes to DOS about 0.1 states/eV at the band center as shown in the inset of Fig. 2(d) for the graphene case ($\alpha = 0$). Therefore, the difference of DOS with and without n_c is negligible. In other words, the broadened flat band suppresses totally the CZEM extension due to either η or n_c. The DOS in Fig. 2 seemingly indicate that the conductivity around $E = 0$ for nonzero α should be much larger than the graphene ($\alpha = 0$) conductivity and the vacancy-disorder-induced CZEM may play a minor role in the affecting transport property because $\sigma(E)$ is generally proportional to the DOS.

IV. BROADENING OF THE FLAT BAND

We first focus on the broadened flat band effect by η, and no vacancy disorder is considered here. The conductivity, $\sigma(E)$ is plotted in Fig. 3(a) within the different parameter α. For the small α case, such as $\alpha = 0.1$, the band center conductivity $\sigma(0)$ has a little enhancement compared with the graphene case ($\alpha = 0$) although the DOS in Fig. 2(a) manifests a significant broadening effect of the flat band. $\sigma_0 = 4e^2/h\pi$ is the universal ZEC value of the graphene. Although for a larger α case, $\alpha = 0.5$ or $\alpha = 1.0$, the conductivity around $E = 0$ significantly increases with a clear conductivity peak in the band center. The larger ZEC undoubtedly comes from the broken flat band, i.e., the original localized electrons in the flat band now contribute to the transport. The same result of the ZEC growth with α was found by considering the evanescent modes contributing to the ZEC [55].

In Figs. 3(b)–3(d), $\sigma(E)$ evolution with the inelastic-scattering strength η is plotted for a fixed α. When $\alpha = 0.1$, $\sigma(E)$ exhibits the Drude conductivity behavior, such as that of graphene, and the ZEC slightly deviates from the minimum σ_0. However, it is not a constant but weakly dependent on η. For the larger α case, $\sigma(E)$ around the band center is significantly increased as shown in Figs. 3(c) and 3(d) for

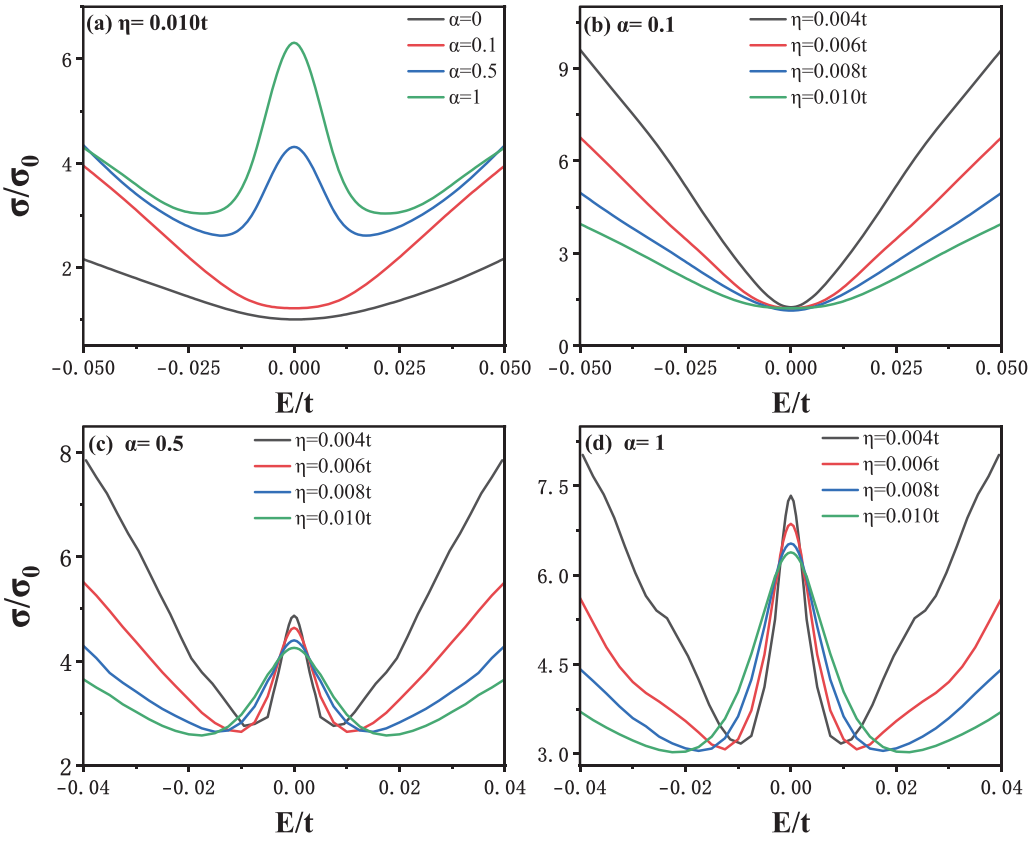

FIG. 3. Low-energy conductivity profiles σ for the nonvacancy disorder case. Parameters are noted in each panel.

$\alpha = 0.5$ and 1.0. Meanwhile, $\sigma(0)$ increases with a decrease in η, and this ZEC peak should be attributed to the broadening effect of the flat band. Slightly away from $E = 0$, there is a narrow energy window in which the system enters into a localized phase because $\sigma(E)$ decreases a lot with a reduction of η. This means $\eta \to 0$ and $\sigma(E) \to 0$ in the clean limit, so the system should be entirely insulating. When E is enhanced further, the system should return to the ballisticlike transport regime, $\sigma(E)$ increases significantly when η decreases.

In Fig. 4, σ as a function of η is plotted in three different typical transport regimes for a fixed $\alpha = 1$. For $E = 0$, the square line indicates that $\sigma(0)$ decreases slightly with η unlike the constant ZEC in graphene. This is, however, consistent with the result in Ref. [41] where the ZEC of the Dice lattice was estimated by self-consistent Born approximation to be $\sigma(0) \sim -\ln \eta^2$, divergent logarithmically as $\eta \to 0$. This metallic property directly originates from the broadening of the flat band because in comparison, graphene exhibits a constant ZEC independent of η without the flat band. The metallic state around $E = 0$ can be dubbed as the supermetallic phase because as $\eta \to 0$, $\sigma(0) \to \infty$, which is very contrasted to the general situation that a 2D system can easily enter into a localized phase [47] when an extremely weak scattering η is introduced.

For the star line in Fig. 4, σ shows a weak increase with η when $E = 0.01t$, which is a typical localization behavior reflecting the electron characteristic of the original flat band. Certainly, the localized energy regime is quite narrow as shown in Figs. 3(c) and 3(d). When the Fermi energy grows further, the system will reenter the ballisticlike transport regime as the triangle line shown in Fig. 4, i.e., the conductivity swiftly decreases with η for $E = 0.04t$ and σ has a Drude trend of $\sigma \sim 1/\eta$.

From Figs. 3 and 4, it is shown that with an increase in α, the flat band would play an increasingly important role in the conductivity behavior for the low-energy transport regime. For instance, the system will transit into the supermetallic phase at $E \sim 0$ from the normal metallic phase at a large α

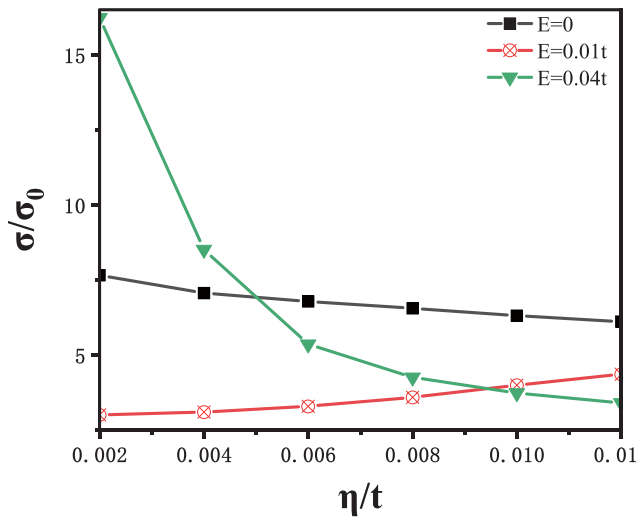

FIG. 4. Conductivity σ versus the inelastic-scattering strength η for the non-vacancy case. $n_c = 0$ and $\alpha = 1$.

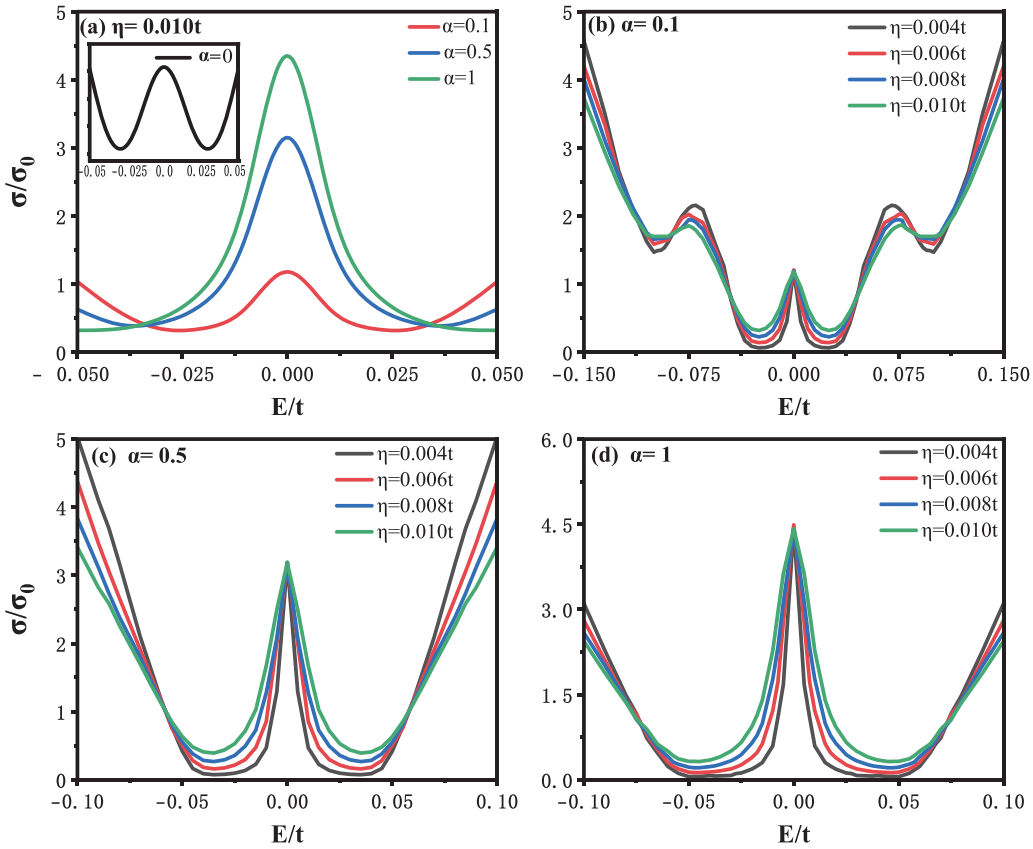

FIG. 5. (a) Conductivity σ as a function of the Fermi energy E for different α's under the vacancy disorder. Evolution of conductivity with η for different α in (b), (c), and (d). The inset of (a) is for the low-energy graphene conductivity $\alpha = 0$. The vacancy density is $n_c = 0.4\%$, and other parameters are marked in each panel.

case, whereas slightly away from $E = 0$, the phase transition from the metallic phase to the localized phase may occur when α increases.

V. DELOCALIZATION OF THE CZEM

In the last section, the broadening of the flat band is shown to enable a supermetallic phase at the band center as well as a nearby localized phase purely due to the inelastic scattering. It is, therefore, quite intriguing to study the delocalization of the CZEM from the vacancy disorder. For one thing, the broadening effect of CZEM on the DOS is totally suppressed by that of the flat band as shown in Fig. 2, and for the other thing, the CZEM was demonstrated to significantly affect the transport properties of the graphenelike Dirac semimetals [42,47,50], e.g., the critical delocalization point of $E = 0$ was identified in those systems.

In Fig. 5, $\sigma(E)$ is calculated with the vacancy density set as $n_c = 0.4\%$. The vacancy is homogeneously distributed among the lattice sites, i.e., the A, B, or C atom in a primitive cell is ticked out and replaced by a vacancy on the same foot. In comparison with Fig. 3(a), the σ magnitude is reduced a little in the case of nonzero n_c. The surprising results are the $\sigma(0)$ peaks appearing even in the small α case, such as $\alpha = 0.1$, which is absent in Fig. 3(a) for the nonvacancy case. For $\alpha = 0$, the graphene case was also shown in the inset of Fig. 5(a), where the ZEC is equal to σ_0.

In Figs. 5(b)–5(d), we present σ versus the Fermi energy E for different η's and α's. It is seen that the conductivity profiles are almost the same: the whole low-energy regime is in the localization phase except the $E = 0$ point where the conductivity remains nearly unchanged for different η's. This indicates that the CZEM dominates the transport property and suppresses the delocalization effect of the flat band. In some sense, the $E = 0$ point is still the critical delocalization point in the vacancy-disordered α-T_3 model. This is the same as other Dirac semimetal systems [47,50] within the vacancy disorder. In addition, the localization regime induced by the CZEM is much wider than that from the flat band in Figs. 3(b)–3(d), e.g. the turning point between the ballistic and localization regime is about $E = 0.075t$ for the $\alpha = 1$ case in Fig. 5(d). For the small α, such as $\alpha = 0.1$, there is a region in which the electrons reenter into the localized regime around $E \sim 0.1t$, this is similar to the self-similar graphene Sierpinski carpet [56] in which fractal structures show the same conductivity behavior including the unified ZEC at the band center.

The conductivity $\sigma(E)$ is plotted as a function of η for $\alpha = 0.1$ and $\alpha = 1.0$ in Fig. 6. It is clearly shown that the ZEC, $\sigma(0)$ keeps little variation with η in both cases, manifesting it as a critical delocalization point. For $E = 0.01t$ in Figs. 6(a) and 6(b), σ increases a little with η reflecting the localized behavior. In the ballistic regime, both $E = 0.05t$ and $E = 0.1t$ curves show that σ is reduced with an increase in

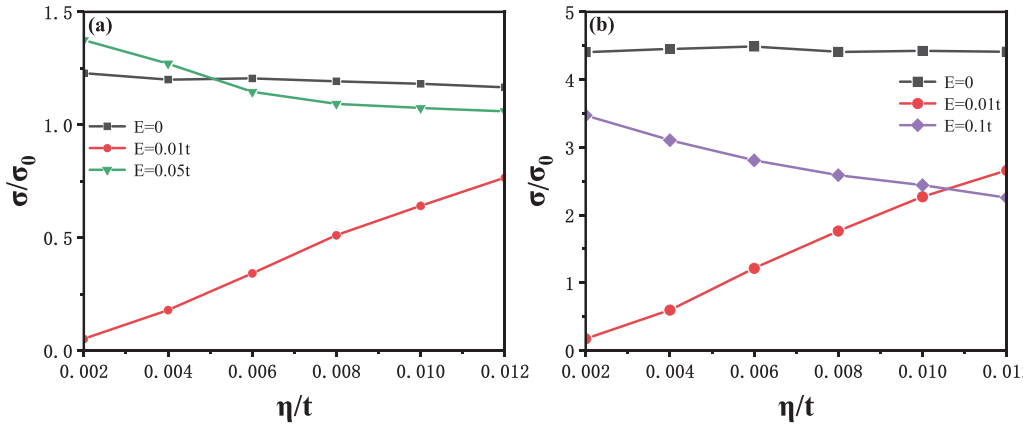

FIG. 6. Conductivity σ versus the inelastic-scattering strength η for $\alpha = 0.1$ in (a) and $\alpha = 1$ in (b). Parameters are marked in each panel.

η. The two cases of $\alpha = 0.1$ and $\alpha = 1.0$ have the similar conductivity behavior in the low-energy regime even though the σ magnitudes have a big difference. This implies that the CZEM is decisive for the vacancy disordered system because no conductivity peak at $E = 0$ for $\alpha = 0.1$ is seen in Fig. 3(a) where the vacancy disorder is absent, and no CZEM exists.

We proceed to study the conductivity dependence on the vacancy density n_c. Generally speaking, the disorder undoubtedly suppresses the conductivity, but the zero-energy critical delocalization point is hardly affected for the BDI-class graphene [47] or chiral-symplectic-class 2D square-bipartite-lattice Dirac semimetals [50]. In Fig. 7, it is shown that the critical point of $\sigma(0)$ has a visible reduction with the vacancy density n_c, whereas the ballistic conductivity ($E = 0.1t$) decreases with n_c a lot. For the localized state, $E = 0.01t$ and $E = 0.02t$, σ shows a clear decrease for a small n_c due to the onset of the induced localization effect of CZEM and then varies smoothly with n_c as seen from the circle-red and triangle-blue lines in Fig. 7(a).

Unlike the mentioned graphene [47] or square-bipartite-lattice semimetals [50], the slight reduction dependence of $\sigma(0)$ on n_c in the studied α-T_3 model should be related to the broadening of the flat band, which is shown to lead to a supermetallic phase at $E \sim 0$ in Fig. 3. The increasing vacancy disorder n_c will further broaden the flat band simultaneously so that it can suppress conductivity at $E = 0$ as the square-black line in Fig. 7(a). In other words, the critical delocalization point in the α-T_3 system is not robust as a result of the existence of the flat band. It is also manifested by the fact that $\sigma(0)$ increases with parameter α as shown in Fig. 7(b) when n_c is fixed since α denotes the weight of the flat band contributing to the electron properties in the system, such as the DOS studied in Fig. 2.

We simply conclude the localization effect dependence on α of electrons in the α-T_3 model in the following. When there is no vacancy in Figs. 3(b)–3(d), the localized region purely due to the broken flat band is enlarged with α, and even no localization effect exists for a smaller α, such as the $\alpha = 0.1$ case in Fig. 3(b). Similarly, the localization regime increases with α in Figs. 5(b)–5(d) when the CZEM is considered, e.g., the turning point for $\alpha = 1$ between the localization and the ballistic regimes is about $E = 0.075t$ whereas it is around $E = 0.04t$ for $\alpha = 0.1$. The larger α is, the more easily the system enters into a localization phase, which agrees with the physics intuitive: the Berry phase is $\gamma = \pi$ for Dirac electrons in graphene unfavorable for localization whereas electrons with $\gamma = 2\pi$ in the Dice lattice ($\alpha = 1$) does not resist localization.

The asymmetric distribution of the vacancy disorder has proven to make a huge difference on the low-energy

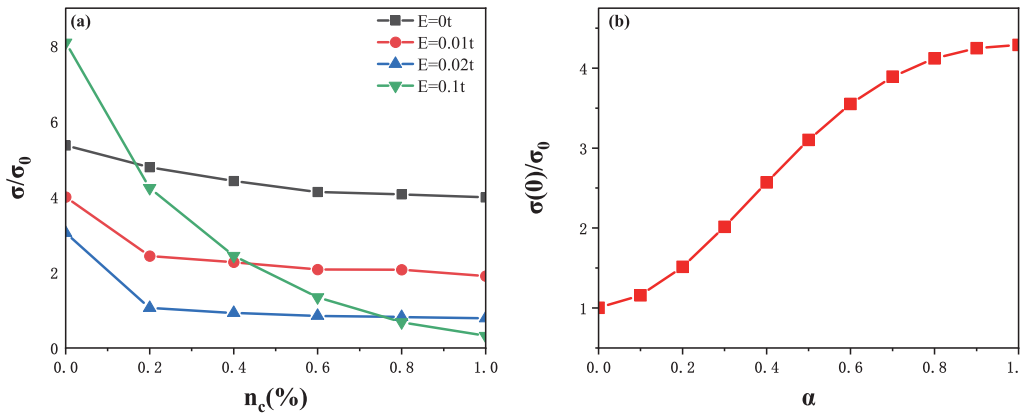

FIG. 7. (a) Conductivity σ as a function of the vacancy density n_c for different Fermi energies and (b) the ZEC as a function of the model parameter α. Parameters are $\eta = 0.01t$, $\alpha = 1$, and $n_c = 0.4\%$.

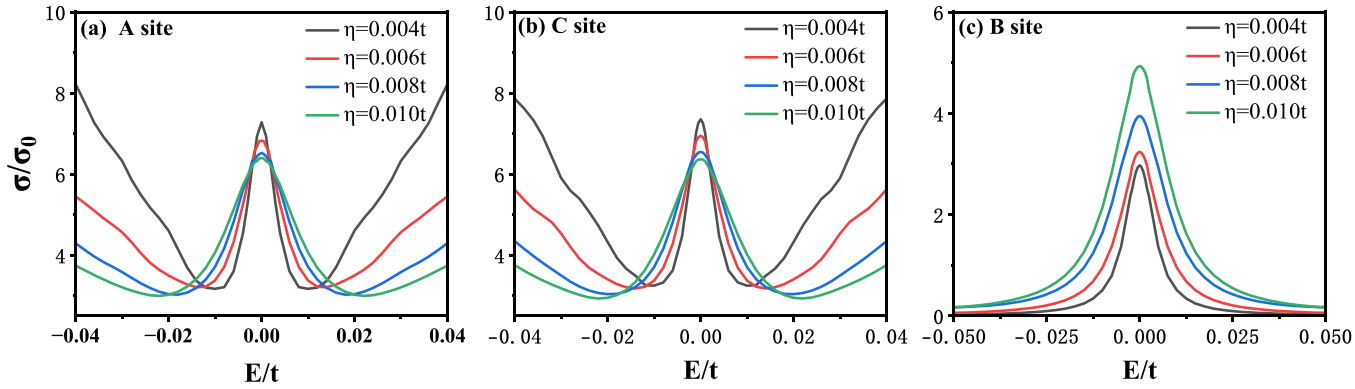

FIG. 8. Low-energy conductivity σ as a function of the Fermi energy E for the vacancy solely residing in the A atom site (a), or the c atom site (b), or the B atom site (c). Parameters are $n_c = 0.4\%$, $\alpha = 1$, and others are marked in panels.

conductivity in other Dirac semimetal systems [50,57], so we also consider this asymmetric vacancy replacement on three A,–C atoms in a primitive cell in Fig. 1(a). The extreme cases are calculated here, and only one of three different ABC atom sites in a primitive cell is replaced by vacancy. When the vacancy is considered only residing at the A atom or the C atom site, the system exhibits a metallic phase in the band center $E \sim 0$ whereas in the adjacent region, σ exhibits a localized behavior as shown in Figs. 8(a) and 8(b). This performance resembles exactly the transport property merely from the broken flat band in Figs. 3(c) and 3(d) without vacancy. In other words, the CZEM effect is removed entirely, and only the broadening effect of the flat band remains. In other Dirac semimetals, such as the 2D square-bipartite lattice [50,57], the extreme imbalance of vacancy generally breaks the inversion symmetry, so an energy gap can occur so as to the generation of a mobility gap. In the studied α-T_3 lattice, either the A site or the C site was replaced the vacancy, the honeycomb lattice structure remains not destroyed severely, so the vacancy can only broaden the flat band, and the CZEM might be suppressed entirely.

When the cental atom B site is replaced by vacancy in Fig. 8(c), the low-energy region is fully localized and even the critical delocalization point $E = 0$ is removed, too. This is a little similar to usual graphene-based [57] or square lattice Dirac semimetal [50] systems where the asymmetric vacancy can remove the critical delocalization point and even generate the mobility gap. Nevertheless, the presence of the broken flat band in the studied α-T_3 lattice prevents the generation of the mobility gap, but instead, the whole low-energy regime is in the localized phase, the conductivity decreases a lot as η is reduced.

VI. CONCLUSION

To summarize, we have investigated the delocalization effect of the CZEM induced by the vacancy disorder and its interplay with the flat band in the α-T_3 lattice model. It is demonstrated that the pure broadening of the flat band will lead to a supermetallic phase at the band center since the ZEC increases weakly with a decrease in the inelastic-scattering strength, whereas a narrow localization regime is identified nearby the band center. When the CZEM due to the vacancy disorder is taken into account, the localized regime is enlarged to the whole low-energy regime except the Dirac point of $E = 0$, which becomes the critical delocalization point because the ZEC is independent of the inelastic-scattering strength. It is also found that the ZEC itself is not a universal value but depends on the model parameter α as well as the vacancy density n_c due to the broadening effect of the flat band. The extreme vacancy imbalance can severely change the critical delocalization scenario from the CZEM that the low-energy regime can be either in the supermetallic phase or the pure localization phase, which depends on whether the central B atom site of a primitive cell is replaced by vacancy or not.

ACKNOWLEDGMENTS

The work was supported by NSFC (Grants No. 12174051 and No. 12174077).

[1] D. Leykam, A. Andreanov, and S. Flach, Adv. Phys. X **3**, 1473052 (2018).
[2] M. Yankowitz, S. Chen, H. Polshyn, Y. Zhang, K. Watanabe, T. Taniguchi, D. Graf, A. Young, and C. Dean, Science **363**, 1059 (2019).
[3] R. W. Havener, Y. Liang, L. Brown, L. Yang, and J. Park, Nano Lett. **14**, 3353 (2014).
[4] S. Dai, Y. Xiang, and D. J. Srolovitz, Nano Lett. **16**, 5923 (2016).
[5] Z. Song, Z. J. Wang, W. J. Shi, G. Li, C. Fang, and B. A. Bernevig, Phys. Rev. Lett. **123**, 036401 (2019).
[6] M. Anđelković, L. Covaci, and F. M. Peeters, Phys. Rev. Mater. **2**, 034004 (2018).
[7] Y. Cao, V. Fatemi, A. Demir, S. Fang, S. L. Tomarken, J. Y. Luo, J. D. Sanchez-Yamagishi, K. Watanabe, T. Taniguchi, E. Kaxiras, R. C. Ashoori, and P. Jarillo-Herrero, Nature **556**, 80 (2018).
[8] Y. Cao, V. Fatemi, S. Fang, K. Watanabe, T. Taniguchi, E. Kaxiras, and P. Jarillo-Herrero, Nature **556**, 43 (2018).
[9] A. Mielke, J. Phys. A **24**, 3311 (1991).
[10] H. Tasaki, Phys. Rev. Lett. **69**, 1608 (1992).
[11] A. Mielke, J. Phys. A **25**, 4335 (1992).

[12] H. Tasaki, Prog. Theor. Phys. **99**, 489 (1998).
[13] M. Imada and M. Kohno, Phys. Rev. Lett. **84**, 143 (2000).
[14] S. Peotta and P. Torma, Nat. Commun. **6**, 8944 (2015).
[15] E. Tang, J.-W. Mei, and X.-G. Wen, Phys. Rev. Lett. **106**, 236802 (2011).
[16] T. Neupert, L. Santos, C. Chamon, and C. Mudry, Phys. Rev. Lett. **106**, 236804 (2011).
[17] S. D. Huber and E. Altman, Phys. Rev. B **82**, 184502 (2010).
[18] C. J. Wu, D. Bergman, L. Balents, and S. Das Sarma, Phys. Rev. Lett. **99**, 070401 (2007).
[19] E. H. Lieb, Phys. Rev. Lett. **62**, 1201 (1989).
[20] B. Sutherland, Phys. Rev. B **34**, 5208 (1986).
[21] R. Shen, L. B. Shao, B. Wang, and D. Y. Xing, Phys. Rev. B **81**, 041410(R) (2010).
[22] N. Goldman, D. F. Urban, and D. Bercioux, Phys. Rev. A **83**, 063601 (2011).
[23] V. Apaja, M. Hyrkas, and M. Manninen, Phys. Rev. A **82**, 041402(R) (2010).
[24] R. A. Vicencio, C. Cantillano, L. Morales-Inostroza, B. Real, C. Mejía-Cortés, S. Weimann, A. Szameit, and M. I. Molina, Phys. Rev. Lett. **114**, 245503 (2015).
[25] D. Guzman-Silva, C. Mejia-Corteés, M. A. Bandres, M. C. Rechtsman, S. Weimann, S. Nolte, M. Segev, A. Szameit, and R. A. Vicencio, New J. Phys. **16**, 063061 (2014).
[26] S. Mukherjee, A. Spracklen, D. Choudhury, N. Goldman, P. Öhberg, E. Andersson, and R. R. Thomson, Phys. Rev. Lett. **114**, 245504 (2015).
[27] J. W. Park, G. Y. Cho, J. Lee, and H. W. Yeom, Nat. Commun. **10**, 4038 (2019).
[28] J. M. Lee, C. H. Geng, J. W. Park, M. Oshikawa, S.-S. Lee, H. W. Yeom, and G. Y. Cho, Phys. Rev. Lett. **124**, 137002 (2020).
[29] A. Wang, X. Zhao, M. Zhao, X. Zhang, Y. Feng, and F. Liu, J. Phys. Chem. Lett. **9**, 614 (2018).
[30] X. Sun, K.-H. Wu, R. Sakamoto, T. Kusamoto, H. Maeda, and H. Nishihara, Chem. Lett. **46**, 1072 (2017).
[31] M. Rizzi, V. Cataudella, and R. Fazio, Phys. Rev. B **73**, 144511 (2006).
[32] J. Vidal, R. Mosseri, and B. Doucot, Phys. Rev. Lett. **81**, 5888 (1998).
[33] J. Vidal, P. Butaud, B. Doucot, and R. Mosseri, Phys. Rev. B **64**, 155306 (2001).
[34] B. Dóra, J. Kailasvuori, and R. Moessner, Phys. Rev. B **84**, 195422 (2011).
[35] F. Wang and Y. Ran, Phys. Rev. B **84**, 241103(R) (2011).
[36] J. D. Malcolm and E. J. Nicol, Phys. Rev. B **92**, 035118 (2015).
[37] E. Illes and E. J. Nicol, Phys. Rev. B **95**, 235432 (2017).
[38] Y. Betancur-Ocampo, G. Cordourier-Maruri, V. Gupta, and R. de Coss, Phys. Rev. B **96**, 024304 (2017).
[39] J. Wang and J. F. Liu, Phys. Rev. B **105**, 035402 (2022).
[40] T. Louvet, P. Delplace, A. A. Fedorenko, and D. Carpentier, Phys. Rev. B **92**, 155116 (2015).
[41] M. Vigh, L. Oroszlány, S. Vajna, P. San-Jose, G. Dávid, J. Cserti, and B. Dóra, Phys. Rev. B **88**, 161413(R) (2013).
[42] G. Bouzerar and D. Mayou, Phys. Rev. B **103**, 075415 (2021).
[43] H.-L. Liu, J. Wang, and J.-F. Liu, Physica E **144**, 115454 (2022).
[44] J. Tworzydło, B. Trauzettel, M. Titov, A. Rycerz, and C. W. J. Beenakker, Phys. Rev. Lett. **96**, 246802 (2006).
[45] G. Trambly de Laissardiere and D. Mayou, Phys. Rev. Lett. **111**, 146601 (2013).
[46] A. Cresti, F. Ortmann, T. Louvet, D. Van Tuan, and S. Roche, Phys. Rev. Lett. **110**, 196601 (2013).
[47] A. Ferreira and E. R. Mucciolo, Phys. Rev. Lett. **115**, 106601 (2015).
[48] V. M. Pereira, F. Guinea, J. M. B. Lopes dos Santos, N. M. R. Peres, and A. H. Castro Neto, Phys. Rev. Lett. **96**, 036801 (2006).
[49] V. M. Pereira, J. M. B. Lopes dos Santos, and A. H. Castro Neto, Phys. Rev. B **77**, 115109 (2008).
[50] L. Liu, Y. Yu, H.-B. Wu, Y.-Y. Zhang, J.-J. Liu, and S.-S. Li, Phys. Rev. B **97**, 155302 (2018).
[51] A. Weisse, G. Wellein, A. Alvermann, and H. Fehske, Rev. Mod. Phys. **78**, 275 (2006).
[52] R. Kubo, J. Phys. Soc. Jpn. **12**, 570 (1957).
[53] D. A. Greenwood, Proc. Phys. Soc., London **71**, 585 (1958).
[54] A. Chandrasekaran and J. J. Betouras, Phys. Rev. B **105**, 075144 (2022).
[55] J. Wang, J. F. Liu, and C. S. Ting, Phys. Rev. B **101**, 205420 (2020).
[56] G. Bouzerar and D. Mayou, Phys. Rev. Res. **2**, 033063 (2020).
[57] P. M. Ostrovsky, I. V. Protopopov, E. J. König, I. V. Gornyi, A. D. Mirlin, and M. A. Skvortsov, Phys. Rev. Lett. **113**, 186803 (2014).